Structure of Ga-Sb-Se glasses by combination of 77 Se NMR and neutron diffraction experiments with molecular dynamics

Eric Furet, Alicia Lecomte, David Le Coq, Fan Zeng, Laurent Cormier, Claire Roiland, Laurent Calvez

Structure of Ga-Sb-Se glasses by combination of ^{77}Se NMR and neutron diffraction experiments with molecular dynamics

Eric Furet[1], Alicia Lecomte[1], David Le Coq[1], Fan Zeng [1], Laurent Cormier [2], Claire Roiland[1], Laurent Calvez[1]

[1]*Univ Rennes, CNRS, ISCR (Institut des Sciences Chimiques de Rennes) – UMR 6226, F-35000 Rennes, France*

[2] *Sorbonne Université, CNRS UMR7590, MNHN, IRD, Institut de minéralogie, de physique des matériaux et de cosmochimie (IMPMC), 4 place Jussieu, F-75005 Paris, France*

**laurent.calvez@univ-rennes1.fr*

Keywords : chalcogenide glass, molecular dynamics, NMR, Neutron diffraction

Abstract

This paper deals with the structural investigation of a new class of glasses belonging to the Ga-Sb-Se system. Neutron diffraction and ^{77}Se NMR were performed on the $Ga_8Sb_{27}Se_{65}$ glass composition to understand the structural network in this unconventional system. The experimental data were confronted to molecular dynamics simulations and show a good agreement. Detailed analyses are consistent with Ga and Se coordination numbers (CN) of 4 and 2, respectively, as usually obtained in chalcogenide glasses. This study also highlights a variable CN of Sb, ranging from 3 up to 5, allowing to better understand the formation of glasses in a such complex system.

Introduction

Chalcogenide glasses (ChG) are known for their optical transparency in the infrared (IR). This quality leads to many applications in various fields such as infrared optics (lenses and fibres), optical data storage, chemical species detection, ionic conductivity [1]... The glasses, currently commercialized, dedicated to the applications in the IR region, are generally made from Germanium (Ge) and / or Arsenic (As) combined with Selenium (Se) to improve the thermomechanical properties. For instance, Gallium (Ga) and Antimony (Sb) can also be added into the Ge-Se system to stiffen the network and to achieve this goal. While Ge is considered to be a network glass former in its Ge-Se form, the entities related to Sb-Se or Ga-Se are considered as network modifiers. The glasses containing these elements are mainly constituted of $GeSe_4$ and $GaSe_4$ tetrahedra as well as $SbSe_{3/2}$ pyramids or $Se_2Sb\text{-}SbSe_2$ structural motifs following the Sb content [1-3]. While the combinations of Ge and Se easily form glasses, the vitreous domain in the Se/Ga or Se/Sb binaries are relatively narrow and occur at very high percentage of Se. Indeed, most of the applications such as photovoltaics based on those binary compounds are generally performed from their crystalline forms Ga_2Se_3 and Sb_2Se_3 [4-6].

This paper is dedicated to the investigation of the structure of recently discovered glasses based on Ga, Sb, and Se [7, 8]. It is indeed paradoxical to form glass in this ternary system since Ga and Sb, added in large proportion in ChG, lead unacceptably to the crystallization of the molten bath and thus to their opacity in the IR range [9]. Consequently, it is interesting to investigate what are the structural characteristics inherent to Sb and Ga, which allow the formation of a vitreous state in this system. In order to determine the structure of the glasses belonging to the Ga-Sb-Se system, the study focuses on the specific $Ga_8Sb_{27}Se_{65}$ composition, which has the highest stability against crystallization [5].

Despite their high level of technological applications, the structure of ChG is still sometimes controversial because of the spectroscopic tools used that let a high degree of liberty in their interpretation. Some progress on the structural network knowledge of these materials are essential to have access to future technological developments. One of the most powerful solution is to combine experimental and theoretical approaches. In the present paper, structural studies performed by neutron diffraction (ND) and ^{77}Se NMR were confronted with first-principles molecular dynamics simulations (MD) to get some clues on the structure at short- and medium-range orders of this new family of glasses. Such complementary investigations in the ChG domain turned out to be very powerful already [10-12].

Experimental details

Glass synthesis

The synthesis of glasses belonging to the Ga-Sb-Se system has been described elsewhere [7]. It is important to point out that all Ga-Sb-Se glasses present a low stability towards crystallization since the empirical factor of stability ΔT corresponding to the difference between the crystallization temperature (Tx) and the glass transition temperature (Tg) is lower than 100°C. The $Ge_8Sb_{27}Se_{65}$ glasses were prepared in a 7mm diameter silica tube. The mixture was progressively heated up to 930°C and then the liquid was melted for 12h. Next, a horizontally quench in water was carried out followed by an annealing for 5h at Tg-20°C (155°C) and a slow slope down to room temperature to lower mechanical constrains.

Characterization technics

The X-ray and neutron diffraction methods give an overall view of the glass structure. The use of locally sensitive spectroscopic methods such as solid-state NMR or Raman spectroscopy is a source of complementary structural information. A first study based on Raman spectroscopy performed on several glasses of this system is presented in our previous paper [7]. This technique allows for understanding the integration of alkali halide within the doped glass structure but does not permit to conclude on the role of Ga or Sb within the Ga-Sb-Se glasses.

^{77}Se (spin I = 1/2) NMR spectra were recorded at room temperature on an Bruker 300 Avance I (7T) spectrometer operating at Larmor frequencies of 57.2 MHz. Spectra were recorded under static and MAS conditions. Then, the spinning frequency was set to 5 kHz. All spectra were acquired due to an Hahnecho pulse sequence, with an echo delay set to 200 µs and 120 µs for static and MAS spectra, respectively. To ensure a full longitudinal relaxation, and thus quantitative spectra, a recycle delay of 350 s was applied [10].

Neutron Diffraction (ND) experiments were performed at room temperature on the 7C2 diffractometer of Orphée reactor (Laboratoire Léon Brillouin – Saclay – France). The glass sample $Ga_8Sb_{27}Se_{65}$ was introduced in a vanadium cell and an incident neutron wavelength of λ = 0.59 Å was used, allowing to cover a *q*-space from 0.32 Å^{-1} up to 18.56 Å^{-1} ($q=4\pi\sin\theta/\lambda$ with 2θ the scattering angle). The accurate incident energy was checked by measuring a nickel reference. The diffracted neutrons were collected during 12 hours under vacuum. The empty vanadium cell and background were also recorded independently in order to correct the initial data. Standard data corrections (detector efficiency, background and container scattering, absorption, multiple scattering, inelastic effects and normalization from a vanadium standard) were applied to obtain the structure factor, *S*(*q*). A Fourier transformation of *S(q)* was applied in order to determine the total pair correlation function *g(r)* using the following equation:

$$g(r) = 1 + \frac{1}{2\pi^2 \rho r} \int_{q_{min}}^{q_{max}} q[S(q) - 1] \sin(qr)\, dq$$

where ρ is the average number density of the glass sample.

Computational details

To build our starting configurations, we relied on the experimental density of the $Ga_8Sb_{27}Se_{65}$ glass composition that was measured to be equal to 5.212 g.cm^{-3}, according to Lecomte *et al* [7]. In order to satisfy the density criterion, 200 atoms were then randomly dispersed in a cubic cell of 17.9 Å^3. All Car-Parrinello molecular dynamics simulations have been performed within the NVT ensemble using the CPMD-3.17.1 package [14, 15] together with Perdew-Burke-Ernzerhof exchange and correlation functionals [16-18]. The plane-wave basis set was expanded up to a kinetic energy cut-off of 25 Ry and the calculations were carried out at the Γ point of the Brillouin zone. The integration step for the simulations was chosen to be equal to 7 a.u. (0.17 fs), and the fictitious electronic mass was taken to be equal to 850 a.u. [17, 18]. The temperature was controlled by means of Nose-Hoover chain thermostats. [19, 20]. Van der Waals interactions were taken into account by means of the empirical Grimme correction G06 [21]. The *in silico* synthesis of the glass was done by starting from initial randomly distributed ionic positions, under the constraint of a minimal distance in order to limit the steep temperature increase due to atomic reorganization. The cell was then first equilibrated in the liquid state (T = 1100 K) for up to 20 ps and subsequently gradually quenched in plateaus of 20 ps separated of 200 K. This leads to a theoretical cooling rate of 10^{13} K.s^{-1}. The statistical averages were then collected at T=300 K for at least 20 ps.

Ionic positions of configurations, taken from the 300K plateau, were optimized. Then, the ^{77}Se NMR parameters were computed using Gauge Including Projected Augmented Wave (GIPAW) formalism [22, 23] as implemented in the CASTEP package, version 18 [24]. The PBE exchange and correlation functional, on-the-fly generated ultrasoft pseudopotentials, and an expansion of the plane-wave basis sets up to an energy cutoff of 500 eV (36.7 Ry) was used. The Brillouin zone was sampled with a 2x2x2 k-points grid. The convergence of the NMR parameters was checked by performing calculations on a sample cell from 400eV up to 600 eV by 50 eV steps.

GIPAW calculations give access to absolute shielding tensors (σ) that are diagonalized to obtain their eigenvalues. The NMR parameters can then be deduced using the following equations:

$$\sigma_{iso} = \frac{1}{3}(\sigma_{xx} + \sigma_{yy} + \sigma_{zz})$$

$$\sigma_{aniso} = \sigma_{zz} - \sigma_{iso}$$

$$\eta = \frac{\sigma_{yy} - \sigma_{xx}}{\sigma_{aniso}}$$

where in the Haeberlen convention [25], $|\sigma_{zz} - \sigma_{iso}| \geq |\sigma_{zz} - \sigma_{iso}| \geq |\sigma_{zz} - \sigma_{iso}|$. Isotropic chemical shift were subsequently calculated using the relation: $\partial_{iso} = \sigma_{ref} - \sigma_{iso}$ where, for σ_{ref}, we used the 1483 ppm value that we successfully employed when investigating ^{77}Se NMR in Ge-Se and Ge-Te-Se glasses [10, 11].

Finally, spectra simulation have been made using Simpson software, that takes into account all previous NMR parameters to emulate experimental spectra [26].

Results and discussion

In this section, we will present the results obtained from molecular dynamics simulations, averaged over three independent trajectories at 300 K. The study focuses on the $Ga_8Sb_{27}Se_{65}$ glass, which is the composition showing the highest stability against crystallization. Figure 1 gathers the various radial distribution functions computed from these trajectories.

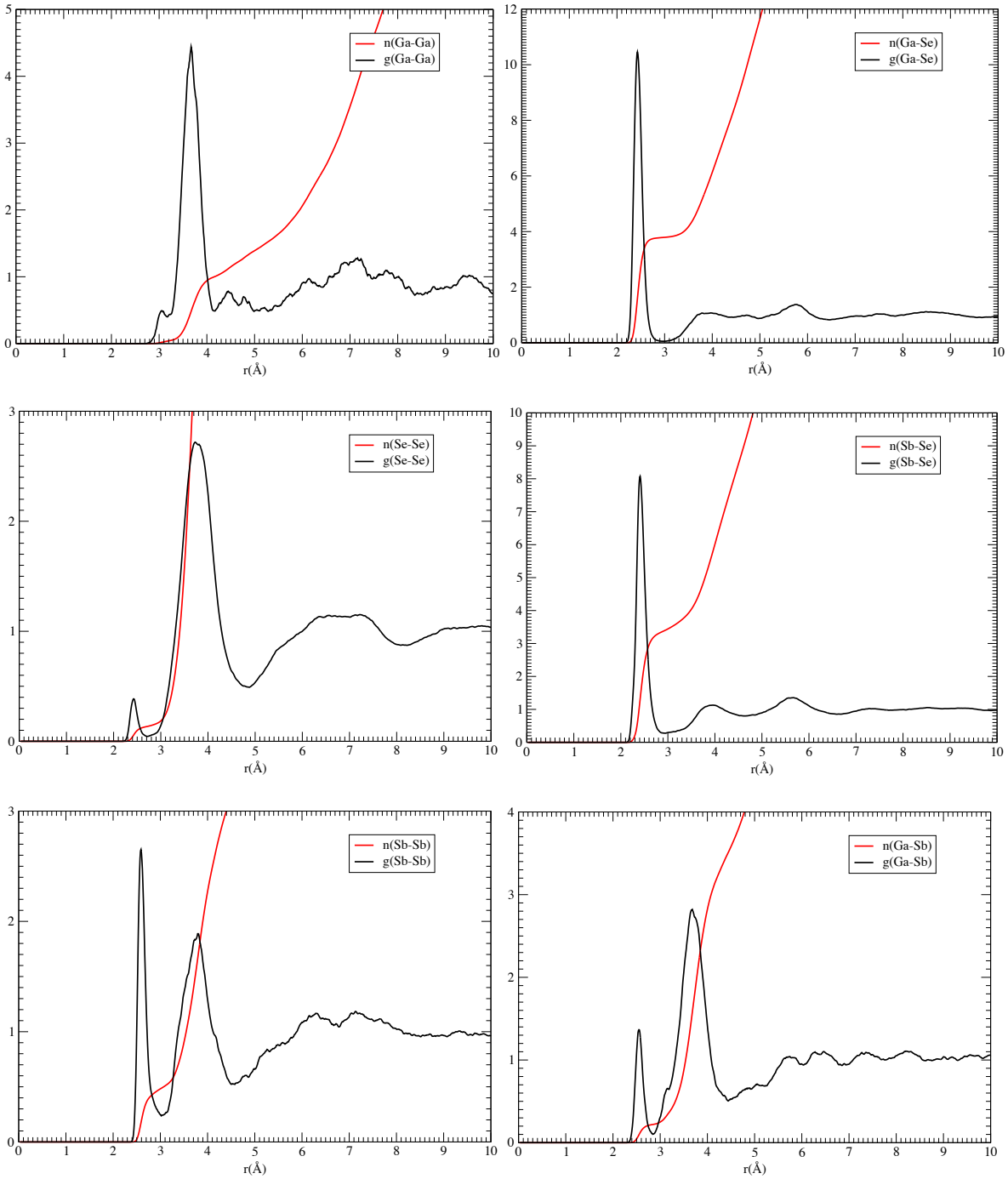

Figure 1 – *Averaged radial distribution functions (black), with their respective integrations functions (red), computed from the three trajectories for the plateaus @300K of our glass model.*

It is immediately seen that the Ga and Se homopolar RDFs exhibit very low values below 3 Å, showing therefore that there is almost or even no Se-Se or Ga-Ga bonds. Table 1 contains the cut-off radii

defining the first coordination spheres, together with values taken from the integrated curves for the corresponding cut-off radii.

Table 1. Cut-off radii (Rc) and number of average neighbor (n) determined @300K for the three molecular dynamics trajectories

	Ga-Ga	Ga-Sb	Ga-Se	Sb-Sb	Sb-Se	Se-Se
Rc(X-Y) (Å)	--	2.8	3.0	3.0	2.9	2.7
n(X-Y)	--	0.2	3.8	0.4	3.4	0.1

The analysis of table 1 shows that Ga atoms possess an average coordination number equal to 4. This result is consistent with previous studies performed on common ChG based on gallium [27, 28]. The main contribution arises from Ga-Se bonds, the integration n(Ga-Se) being equal to 3.8, with a remaining minor contribution coming from Sb, since there is no homopolar Ga bond. Se atoms corresponding to 65 at. % of the investigated composition tend therefore to isolate Ga and hence to prevent the formation of Ga-Sb bonds. Similar conclusions can be drawn for Sb, since we obtain an average coordination number that is close to 4, with a large fraction of Sb-Se bonds. It should be noted that we have however here a small contribution from homopolar Sb-Sb bonds (n(Sb-Sb) = 0.4). As such, the first crude picture of this glass composition taken from molecular dynamics calculations, consists in building blocks consisting of $GaSe_{4/2}$ et $Sb(Se/Sb)_{4/2}$ (averaged) structural units.

A finer picture can be deduced on the basis of the distribution of coordination for each atom type as depicted in figure 2.

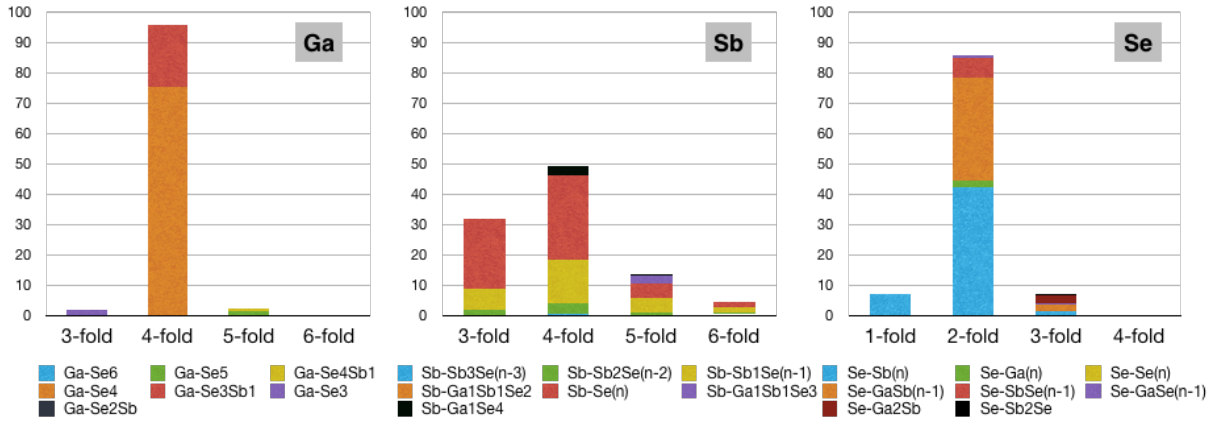

Figure 2- *Averaged distribution of coordination modes for the three atom types calculated from the three plateaus @300K for our glass model.*

These histograms unambiguously confirm the tetra- and bicoordinated mode of Ga and Se, with values of 95% and 85%, respectively. For Ga specifically, the $GaSe_{4/2}$ structural units solely amount to 76% with 20% of $Ga(Se_3Sb)$ additional building blocks. Concerning Se atoms, they are mostly bridging Sb coordination polyhedra through Sb-Se-Sb units (43%), as well as, gallium and antimony atoms by means of Ga-Se-Sb interconnecting units (34%). It should be pointed out that no significant percentage of Ga-Se-Ga bridging units could be found, probably due to the low fraction of Ga. Taken as a whole, these features explain therefore the low fraction of Se-Se homopolar bonds found, despite the dominant fraction of this chalcogen in the investigated glasses. Indeed, we obtain at best 7% of Se-Se-Sb units.

Concerning antimony, the analysis of its coordination mode histogram shows that the situation is more complex than anticipated on the basis of the radial distribution functions that were suggesting the existence of $Sb(Se/Sb)_{4/2}$ polyhedra. We compute indeed a much broader variety of Sb structural units ranging from tri-, tetra-, and pentacoordination modes with percentages of 30, 50, and 13%, respectively. We note that the expected triangular SbX_3 unit can be found, but it is not predominant. For each SbX_n (n = 3-5) type, selenium appears to be the major constituent of the coordination sphere, with values of 23, 28, and 6%. Next, in decreasing order comes antimony with a total percentage among all coordination SbX_n modes of 31%, that leading therefore to significant fraction of Sb-Sb homopolar bonds. The preference to form polar bonds is qualitatively consistent with the expected increased stability related to electrostatic interaction due to the partial ionic character of a heteronuclear bond. For example, the dissociation energy of a Ga-Ga bond amounts for 138 kJ/mol, while for Ga-Sb, it reaches 209 kJ/mol. Given the lack of dissociation energy data for a Ga-Se, we report the one of Ga-Te, with a less electronegative atom and that is expected to exceed 250 kJ/mol [29].

Figure 3 contains the Se-Ga-Se and Se-Sb-Se angular distribution functions (ADF), that correspond to predominant environments in our glass model. It is immediately seen that Ga coordination mode is mostly tetrahedral, with the Se-Ga-Se ADF centered around 109°. The Se-Sb-Se ADF is less clearly defined with a maximum extending from 90 to 115°. A secondary maximum can be noted around 175°. This result is not completely surprising given the much larger diversity of coordination modes (3, 4 and even 5 coordinated) observed for antimony. The computed ADF suggests that not only tetrahedral environment is present, but also some fractions of square or triangular bipyramids. Finally, we may assume that trigonal planar $SbSe_3$ entities are responsible for the shoulder at 120° in the Se-Sb-Se ADF.

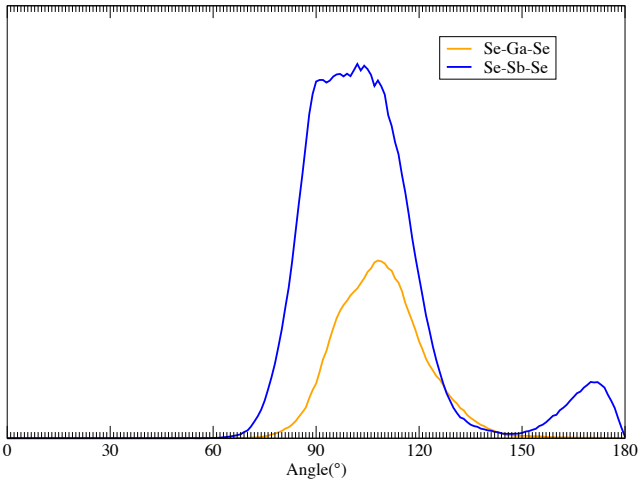

Figure 3- *Averaged Angular distribution function (°) for Se-Sb-Se (blue) and Se-Ga-Se (orange) computed from the three plateaus @300K.*

Most of the findings given below can be seen in the snapshot of our $Ga_8Sb_{27}Se_{65}$ glass model extracted from a 300 K plateau, given in Figure 4. The MD snapshot shows that the structuration of the glass is rather homogeneous. A visualization obtained by discarding the Sb atoms clearly shows the dispersion of gallium in the selenium matrix, hence the lack of any homopolar bonds, the tetrahedral environment for Ga, and the presence of few polyhedra interconnected by Ga-Se-Ga sequence. A similar task, discarding only the Ga atoms, shows unambiguously the richness of the antimony environment, the rather large fraction of Sb-Sb homopolar bonds. It should be pointed out that the presence of a structure containing several Sb-Sb units that can be detected in Figure 4, may suggest some tendency to form antimony aggregates.

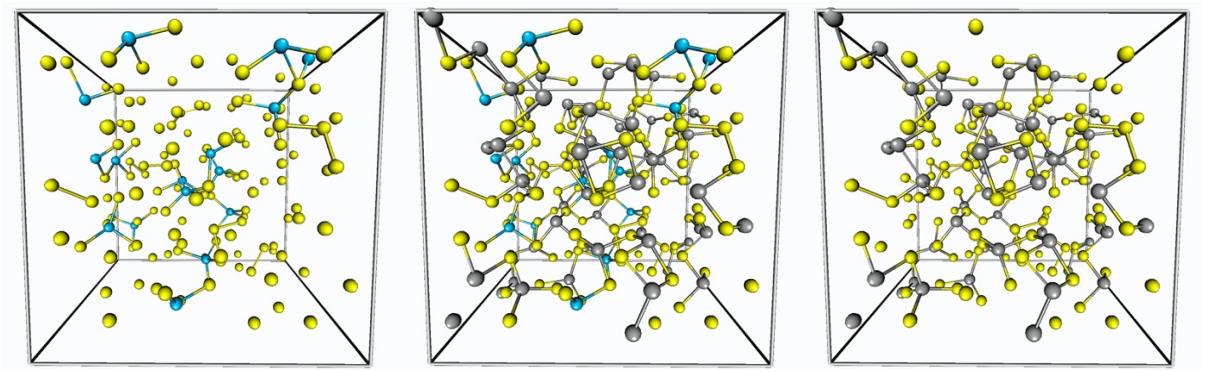

Figure 4. Visualization of $Ga_8Sb_{27}Se_{65}$ glass (middle), Sb (grey), Se (yellow), Ga (cyan), together with two views in which Sb (left) and Ga (right) are discarded for the sake of clarity.

Turning to an analysis in the reciprocal space, Figure 5-a shows the experimental and theoretical neutron structure factors. It is immediately seen that the position of the various extrema are correctly displayed for q values above 2.0 A^{-1}. We note around 1.0 A^{-1} on the theoretical curve, the presence of the so-called "First Sharp Diffraction Peak" (FSDP) that is considered as a typical feature of chalcogenide glasses. It is associated to the intermediate order structuration of the glass, *i.e.* for the second to third coordination sphere [30, 31]. This FSDP is also present in the experimental signal, but the agreement on the position with the computed one is less accurate probably due to the limited size of our simulation cell. The agreement is also somewhat less satisfactory with respect to the height of the first maxima. Indeed, the first maximum around 2.0 A^{-1} is lower than the experimental one, while the second is higher. Minima in the 2.0-5.0 A^{-1} are deeper than their experimental counterparts. Taken as a whole the agreement is quite good and this gives some further credit to our model glass obtained by molecular dynamics.

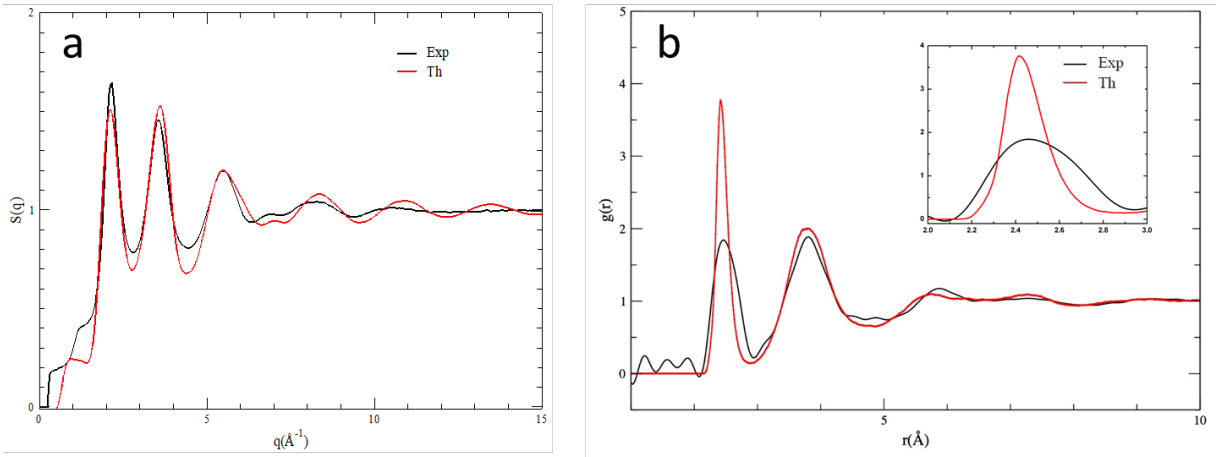

Figure 5. (a) Total neutron structure factors *S(q)* and (b) total pair correlation functions *g(r)* for $Ga_8Sb_{27}Se_{65}$ glass composition. Experimental and theoretical data are in black and red, respectively. The inset graph emphasizes on the *r*-range between 2 and 3 Å.

Next, a comparison of the experimental and calculated total pair correlations is shown in figure 5-b. At first, we can clearly observe that both data are in good agreement even if some differences in the intensity of the peak can be underlined. The position of the first neighboring is located at $r \approx 2.41$ Å and $r \approx 2.43$ Å for theoretical and experimental data, respectively. The second main contribution corresponding to the second neighbors is centered at $r \approx 3.80$ Å in the two cases. The observed widening of the first coordination sphere in the experimental *g(r)* could be originated from two

reasons. At first, to obtain the real-space information with the better resolution, it is important to measure *S(q)* in the highest *q*-range with a large q_{max}. In our experiments the *q*-range spreads from 0.32 $Å^{-1}$ up to 18.56 $Å^{-1}$ meaning that the resolution is not optimized. Nevertheless, another reason is assumed since a marked shoulder is observed at $r \approx 2.68$ Å as observed in the inset of the figure 5-b. In other words, a correlation, not really pointed out at this distance in the theoretical *g(r)*, exists. As a matter of fact, taking into account the composition and the covalent radii of Ga, Se, and Sb (1.26 Å, 1.17 Å, and 1.38 Å, respectively), the probability that this contribution can be attributed to the Sb-Sb correlations is strong. This assumption is also supported by the averaged radial distribution function Sb-Sb exhibited in figure 1 in which its correlation is highlighted, even if a light *r*-shift appears between the two data sets.

Figure 6 shows ^{77}Se solid-state NMR spectra obtained under static and MAS conditions. Both spectra present an asymmetric signal, due to a shallow shoulder on the strong chemical shift values side, centered at approximatively 450 ppm. The width of the measured NMR signal is equal to approximatively 70 kHz under both conditions. The broadening is not affected by MAS. So, the linewidth is only due to a distribution of chemical environments and not to chemical shift anisotropy, meaning, it is only characteristic of the disorder of the glassy network. A simulated spectrum using Simpson on the basis of the calculated NMR parameters obtained within the GIPAW formalism, together with the decomposition of the total signal into the various contributions arising from the different selenium bicoordinated sequences (X-Se-Y; X, Y = Se, Ga, Sb) is also plotted on figure 6. We note an overall agreement between theory and experiment spectra, despite the rather featureless ^{77}Se NMR signal, something that is not surprising in (chalcogenide) glass NMR [10, 32].The maximum of the experimental data and the one obtained theoretically are both close to 200 ppm. The theoretical signal extends over chemical shift spanning from -500 to 1500 ppm, which is a range slightly overestimated with respect to the experimental lineshape that can be considered to be limited from -300 to -1000 ppm. We have already observed such an overestimation of the chemical shift when investigating other ChG, but it does not affect the analysis of the material [11, 12].

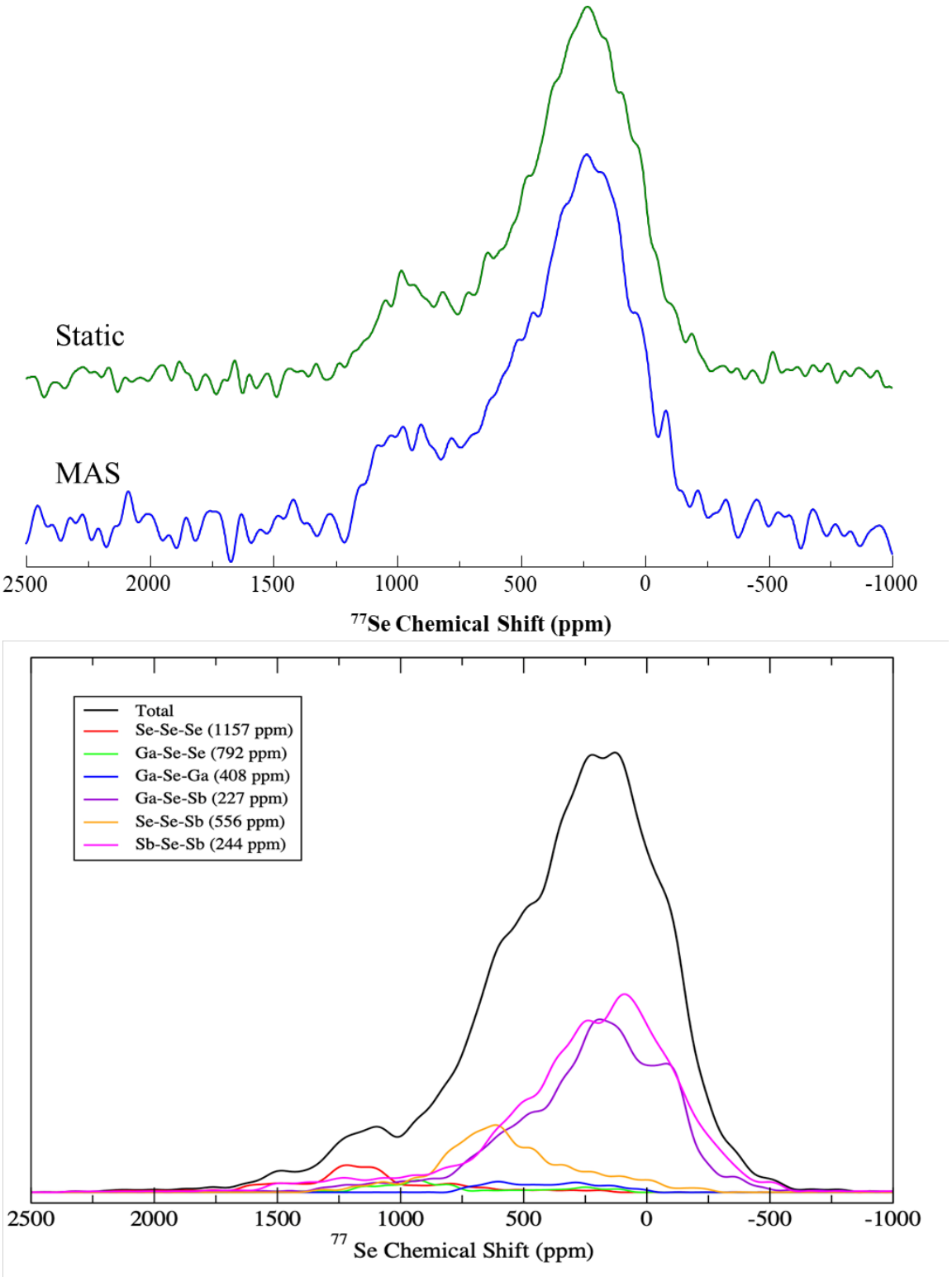

Figure 6. Static and MAS experimental ^{77}Se NMR spectra (top) and MAS simulated one (bottom) on an optimized configuration taken from the 300K plateaus of the $Ga_8Sb_{27}Se_{65}$ glass composition. Contributions of various environments are given together with their mean ∂_{iso} values.

An in-depth analysis of the theoretical ^{77}Se NMR spectrum on the basis of the individual X-Se-Y sequences shows that major contributions arise from Sb-**Se**-Sb and Ga-**Se**-Sb units, with average values

corresponding to 244 ppm and 227 ppm, respectively. Those two types of bicoordinated selenium atoms, that interconnects Sb or Ga/Sb polyhedra, contribute almost equally to the right-hand side of the NMR signal. A secondary contribution related to Se-**Se**-Sb sequences, centered at 556 ppm is to some extent responsible of the observed asymmetry of the signal. Finally, we note that a much weaker contribution can be detected corresponding to stronger deshielding, associated to the rare case of selenium chains units (Se-**Se**-Se). Despite the very low fraction of Se-Se-Se in our simulation cell, the corresponding average chemical shift displacement is calculated to be close to 1100 ppm, a value that is quite consistent with the 900 ppm measured for crystalline Se [32]. We note that residual contributions associated to the very few Ga-**Se**-Ga and Se-**Se**-Ga units have no significant impact on the overall shape of the peak, because they overlap with the two Sb-**Se**-Sb and Ga-**Se**-Sb main contributions and may therefore be discarded.

Finally, it should be pointed out that the observed evolution of the average ^{77}Se chemical shift displacement is consistent with the (de)shielding capability of its first neighbors. Indeed, an examination of Table 2, shows that substituting one selenium by a less electronegative element like Ga or Sb induces an increase of shielding (upfield shift) of the ^{77}Se nucleus and hence of the chemical shift values. We observe that the impact of gallium with respect to antimony seems more limited despite its lower electronegativity with respect to Sb, but also possesses a much smaller electron cloud. In fact, switching from Se-Se-Se to Se-Se-Sb sequence induces a drop of chemical shift values of ~600 ppm. Substituting the remaining Se atom by Sb or Ga to obtain Ga/Sb-Se-Sb units lead to additional decrease, with calculated δ_{iso} values close to 230-250 ppm. It should be noted that even for the very rare sequences, namely Se-Se-Ga and Ga-Se-Ga, for which the conclusions can obviously not be considered as statistically pertinent, the impact of first neighbor holds (Table 2).

Table 2. Averaged isotropic chemical shifts *(δ_{iso}, ppm) and total number of sites (N) for each type of X-Se-Y (X,Y = Ga,Se,Sb) units in our glass model.*

X-Se-Y environment	δ_{iso}	N
Se-Se-Se	1157	5
Se-Se-Sb	556	13
Sb-Se-Sb	244	50
Ga-Se-Se	792	2
Ga-Se-Sb	227	40
Ga-Se-Ga	408	2

Taken as a whole, the comparison of experimental total neutron structure factor and ^{77}Se NMR spectrum with the theoretical ones give credits to our glass model obtained by molecular dynamics.

Conclusion

The structure of a $Ga_8Sb_{27}Se_{65}$ glass was investigated using neutron diffraction and ^{77}Se NMR. The experimental results were compared to MD simulations using a box of 200 atoms. Both experimental and theoretical data present a good agreement validating the glass model obtained by molecular dynamics and allowing extraction of structural information, especially concerning the local arrangement around each element.

In this intriguing glass, one can consider that Se atoms are mostly interconnected to Sb forming polyhedra through Sb-Se-Sb units, as well as, gallium and antimony atoms by means of Ga-Se-Sb

interconnecting units. Some residual Sb-Sb homopolar bonds are also observed due to the high quantity of Sb present within the glass.

While Ga and Se atoms possess an average coordination number equal to 4 and 2, respectively, as expected, a much broader variety of Sb structural units ranging from tri-, tetra-, and pentacoordination can be observed. This result is also confirmed with computed angular distribution functions.

Glasses belonging to the Ga-Sb-Se system present a high tendency to crystallize with ΔT, difference between the crystallization temperature and the glass transition temperature, below 100°C. This study shows that the variety of coordination number of antimony gives flexibility to the network to form amorphous material. Understanding this point, chemical compositions can be optimized to control the crystallization kinetics of the material. The good agreement achieved between theoretical and experimental data during the current investigation performed on the most stable composition of the Ga-Sb-Se system paves the way for further studies on related compositions in an attempt to try to rationalize the stability of this family of glasses towards crystallization.

Acknowledgments

Authors would like to acknowledge the IUF (Institut Universitaire de France) for their financial support. This work was granted access to the HPC resources of CINES under the allocation **A0040807418** made by GENCI (Grand Equipement National de Calcul Intensif).

References

[1] Springer Handbook of Glass, Springer International Publishing, 2019.
[2] M. Olivier, J.C. Tchahame, P. Němec, M. Chauvet, V. Besse, C. Cassagne, G. Boudebs, G. Renversez, R. Boidin, E. Baudet, V. Nazabal, Structure, nonlinear properties, and photosensitivity of (GeSe2)100-x(Sb2Se3)x glasses, Opt. Mater. Express, 4 (2014) 525-540.
[3] E. Petracovschi, L. Calvez, L. Cormier, D.L. Coq, J. Du, Short and medium range structures of 80GeSe2–20Ga2Se3chalcogenide glasses, Journal of Physics: Condensed Matter, 30 (2018) 185403.
[4] R. Babaeva, Structural and Optical Properties of Ga2Se3 Crystals by Spectroscopic Ellipsometry, Journal of Electronic Materials, 48 (2019) 2418–2422.
[5] Y. Wang, J. Li, Y. Chen, J. Zhou, J. Zhang, W. Mao, S. Zheng, Y. Pan, Y. Liu, K. Dai, X. Hu, J. Tao, G. Weng, J. Jiang, S. Chen, J. Chu, Effects of working pressure and power on photovoltaic and defect properties of magnetron sputtered Sb2Se3 thin-film solar cells, Applied Optics, 59 (2020) 948-954.
[6] Z. Li, X. Liang, G. Li, H. Liu, H. Zhang, J. Guo, J. Chen, K. Shen, X. San, W. Yu, R.E.I. Schropp, Y. Mai, 9.2%-efficient core-shell structured antimony selenide nanorod array solar cells, Nature Communications, 10 (2019) 125.
[7] A. Lecomte, V. Nazabal, D. Le Coq, L. Calvez, Ge-free chalcogenide glasses based on Ga-Sb-Se and their stabilization by iodine incorporation, Journal of Non-Crystalline Solids, 481 (2018) 543-547.
[8] Woodhead Publishing Series in Electronic and Optical Materials, in: J.-L. Adam, X. Zhang (Eds.) Chalcogenide Glasses, Woodhead Publishing, 2014, pp. xvii-xxi.
[9] L. Calvez, P. Lucas, M. Rozé, H.L. Ma, J. Lucas, X.H. Zhang, Influence of gallium and alkali halide addition on the optical and thermo–mechanical properties of GeSe2-Ga2Se3 glass, Applied Physics A, 89 (2007) 183-188.
[10] K. Sykina, B. Bureau, L. Le Pollès, C. Roiland, M. Deschamps, C.J. Pickard, E. Furet, A combined 77Se NMR and molecular dynamics contribution to the structural understanding of the chalcogenide glasses, Physical Chemistry Chemical Physics, 16 (2014) 17975-17982.

[11] L. Bouëssel du Bourg, C. Roiland, L. le Pollès, M. Deschamps, C. Boussard-Plédel, B. Bureau, C.J. Pickard, E. Furet, Impact of Te on the structure and 77Se NMR spectra of Se-rich Ge–Te–Se glasses: a combined experimental and computational investigation, Physical Chemistry Chemical Physics, 17 (2015) 29020-29026.
[12] L. Bouëssel Du Bourg, E. Furet, A. Lecomte, L. Le Pollès, S. Kohara, C.J. Benmore, E. Bychkov, D. Le Coq, Experimental and Theoretical Insights into the Structure of Tellurium Chloride Glasses, Inorganic Chemistry, 57 (2018) 2517-2528.
[13] D. Massiot, F. Fayon, M. Capron, I. King, S. Le Calvé, B. Alonso, J.-O. Durand, B. Bujoli, Z. Gan, G. Hoatson, Modelling one- and two-dimensional solid-state NMR spectra, Magnetic Resonance in Chemistry, 40 (2002) 70-76.
[14] R. Car, M. Parrinello, Unified Approach for Molecular Dynamics and Density-Functional Theory, Physical Review Letters, 55 (1985) 2471-2474.
[15] D. Marx, J. Hutter, Ab Initio Molecular Dynamics: Basic Theory and Advanced Methods, Cambridge University Press, Cambridge, 2009.
[16] J.P. Perdew, K. Burke, M. Ernzerhof, Generalized Gradient Approximation Made Simple, Physical Review Letters, 77 (1996) 3865-3868.
[17] N. Troullier, J.L. Martins, Efficient pseudopotentials for plane-wave calculations. II. Operators for fast iterative diagonalization, Physical Review B, 43 (1991) 8861-8869.
[18] N. Troullier, J.L. Martins, Efficient pseudopotentials for plane-wave calculations, Physical Review B, 43 (1991) 1993-2006.
[19] S. Nosé, A molecular dynamics method for simulations in the canonical ensemble, Molecular Physics, 52 (1984) 255-268.
[20] W.G. Hoover, Canonical dynamics: Equilibrium phase-space distributions, Physical Review A, 31 (1985) 1695-1697.
[21] S. Grimme, Semiempirical GGA-type density functional constructed with a long-range dispersion correction, Journal of Computational Chemistry, 27 (2006) 1787-1799.
[22] C.J. Pickard, F. Mauri, All-electron magnetic response with pseudopotentials: NMR chemical shifts, Physical Review B, 63 (2001) 245101.
[23] J.R. Yates, C.J. Pickard, F. Mauri, Calculation of NMR chemical shifts for extended systems using ultrasoft pseudopotentials, Physical Review B, 76 (2007) 024401.
[24] S.J. Clark, M.D. Segall, C.J. Pickard, P.J. Hasnip, M.J. Probert, K. Refson, M.C. Payne, First principles methods using CASTEP, Zeitschrift für Kristallographie, 220 (2005) 567-570.
[25] U. Haeberlen, High resolution NMR in solids : selective averaging / Ulrich Haeberlen, Academic Press, New York, 1976.
[26] M. Bak, J.T. Rasmussen, N.C. Nielsen, SIMPSON – An important driver for numerical simulations in solid-state NMR spectroscopy, Journal of Magnetic Resonance, 213 (2011) 401-403.
[27] A.W. Mao, B.G. Aitken, R.E. Youngman, D.C. Kaseman, S. Sen, Structure of Glasses in the Pseudobinary System Ga2Se3–GeSe2: Violation of Chemical Order and 8-N Coordination Rule, The Journal of Physical Chemistry B, 117 (2013) 16594-16601.
[28] R. Golovchak, L. Calvez, E. Petracovschi, B. Bureau, D. Savytskii, H. Jain, Incorporation of Ga into the structure of Ge–Se glasses, Materials Chemistry and Physics, 138 (2013) 909-916.
[29] https://labs.chem.ucsb.edu/zakarian/armen/11---bonddissociationenergy.pdf, in.
[30] S.R. Elliott, Origin of the first sharp diffraction peak in the structure factor of covalent glasses, Physical Review Letters, 67 (1991) 711-714.
[31] S.R. Elliott, Medium-range structural order in covalent amorphous solids, Nature, 354 (1991) 445-452.
[32] B. Bureau, J. Troles, M. LeFloch, F. Smektala, G. Silly, J. Lucas, Solid state 77Se NMR investigations on arsenic-selenium glasses and crystals, Solid State Sciences, 5 (2003) 219-224.